Cyclic Behavior of Buckling-Restrained Braces for Ductile End Cross Frames

LYLE P. CARDEN, AHMAD M. ITANI, and IAN G. BUCKLE

Damage to the superstructure of steel plate girder bridges during previous earthquakes (Astaneh-Asl, Bolt, McMullin, Donikian, Modjtahedi, and Cho, 1994; Shinozuka, Ballantyne, Borcherdt, Buckle, O'Rourke, and Schiff, 1995; Bruneau, Wilson, and Tremblay, 1996), has highlighted the need to reduce the effects of transverse seismic loading and, at the same time, indicated a means of achieving this objective with the use of ductile end cross frames (Zahrai and Bruneau, 1998, 1999). By designing the cross frames for ductile behavior, the transverse base shear in a bridge can be reduced, minimizing damage to the substructure and other critical superstructure components. Furthermore, confining damage to purpose-built ductile elements that can be easily replaced after an earthquake may reduce the need for bridge closures following a major earthquake.

Past work (Carden, Itani, and Buckle, 2006a) describes component and shake table experiments on a two-girder bridge with single-angle X-brace frames and confirms that with good connection details, these simple braces are able to significantly reduce the base shear. They are maintenance-free, inexpensive, simple to install, and have a large deformation capacity. However, large transverse displacements (drift) may occur in the superstructure as a consequence of the plastic elongation in the brace when in tension, and buckling in compression resulting in suboptimal energy dissipation characteristics during repeated loading. Unless provisions are made for these drifts, structural distress may occur in the slab-to-girder connections or in the girders themselves.

Lyle P. Carden is a post-doctoral research scholar, department of civil and environmental engineering, University of Nevada, Reno, NV.

Ahmad M. Itani is associate professor, department of civil and environmental engineering, University of Nevada, Reno, NV.

Ian G. Buckle is professor, director of center for civil engineering earthquake research, department of civil and environmental engineering, University of Nevada, Reno, NV.

Furthermore, serviceability requirements immediately following an earthquake mean that minimum levels of residual strength and stiffness must be maintained, even though the braces are secondary members with respect to gravity loads (in a straight bridge). This requirement is difficult to guarantee with buckled members. Thus, many of the X-braces will need replacement following an earthquake.

To address the limitations of angle members (suboptimal energy dissipation, uncertain residual stiffness, and member replacement), an end cross frame with the same or better energy dissipation at less drift, with reliable post-earthquake stiffness and strength and a low likelihood of need for replacement, is desired. For this reason, the use of buckling-restrained braces (BRB), instead of the angle members, has been investigated, and the results are reported in this paper.

One example of a BRB is the "unbonded" brace, developed and manufactured by Nippon Steel Corporation in Japan (Wada, Saeki, Takeuchi, and Watanabe, 1989), as illustrated in Figure 1. These braces are constructed from a cruciform or rectangular steel core of specially formulated, low-yield-point steel. The core is surrounded by a debonding material and encased in a steel hollow tube filled with grout. The debonding material allows the core to slide rela-

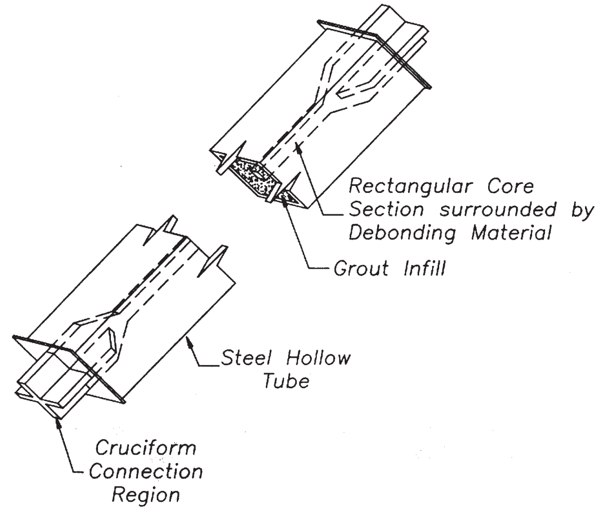

Fig. 1. Buckling-restrained brace.

tive to the encasement. Unbonded braces used in large-scale bridge experiments (Figure 2) were shown to improve the energy dissipation in the end cross frames compared with X-braces and, as degradation in stiffness is prevented, they were less likely to require replacement soon after an earthquake, as is necessary for single-angle X-braces (Carden et al., 2006a).

Buckling-restrained braces designed for use in end cross frames of bridges are typically much smaller, with shorter core lengths, than those used for concentrically braced frames in buildings. The objective of this paper is to evaluate the inelastic cyclic axial behavior of braces as proposed for use in ductile end cross frames of steel girder bridges. Different loading histories, including slow-cyclic and dynamic-cyclic loading were investigated.

EXPERIMENTAL SETUP

Experiments were performed on seven buckling-restrained braces, provided by Nippon Steel Corporation, termed "unbonded" braces. Four of the braces were used solely for axial cyclic experiments, while the remaining three were used in shake table experiments on the large-scale bridge model before being tested to failure using cyclic axial loads. Axial experiments were performed to evaluate overall brace behavior, cumulative displacement capacity, effect of different loading histories, and effect of dynamic loading. Loads were applied to the braces using the load frame shown in Figure 3. The dimensions and connection configurations for the braces are illustrated in Figure 4. Experiments were performed on the first brace with pin-ended connections between the gusset plate and the load frame grips as shown in Figures 4a and 5, while the remaining braces used bolted, moment-resisting connections, which were designed to be slip critical based on the serviceability criteria in the AISC *Load and Resistance Factor Design Manual of Steel Construction* provisions (AISC, 2001) (Figures 4b and 6). The pin-ended connection was intended to prevent bending moments in the brace. To minimize the size of the fixed slip-critical connection, two rows of bolts were used to connect the brace in the direction of larger core plate dimension (in the plane of the end cross frame in the bridge model), while the perpendicular legs of the cruciform connection were connected with a single row of bolts at each interface. The force at which slippage was expected to occur was equal to 40.1 kips, which was approximately two times the expected yield strength of the brace. The total length of the brace was equal to $38\frac{1}{8}$ in., including the connection regions on the cruciform section (Figure 3). The core length was equal to $20\frac{3}{8}$ in. between the centers of the transition between the maximum cruciform and minimum core sections at either end of the brace. The cross-sectional dimensions of the core plate were 1 in. $\times$ $\frac{5}{8}$ in.

Fig. 2. Large-scale steel plate girder bridge model with buckling-restrained braces in the end cross frames.

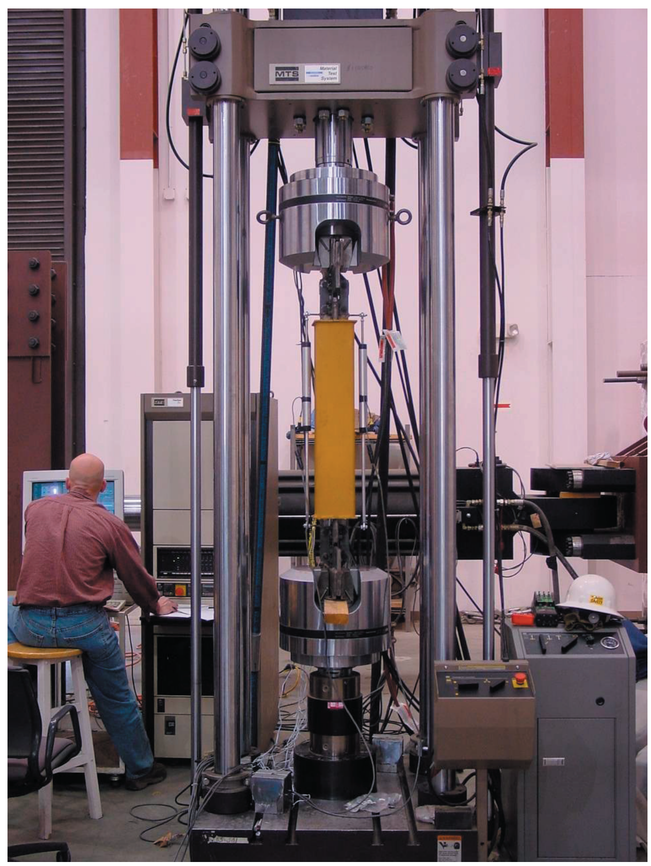

Fig. 3. Load frame for applying reversed cyclic axial loads to the buckling-restrained braces.

Three of the unbonded braces were instrumented with strain gages to measure strains on each side of the plate at each end of the core length. The braces were also instrumented with two displacement transducers on either side of the brace to measure displacements across the core length of the brace as shown in Figure 3. The displacement across the entire length of the brace, including connection regions, was also measured using the actuator, and the axial force was measured by the actuator load cell.

The loading history for each of the braces differed. Brace A was subjected to a modified ATC 24 loading history (ATC, 1992). The modification involved subjecting the brace to two cycles at each excursion instead of three cycles as in ATC 24. The history was based on the applied force until yielding occurred, then increased based on the displacement at yield. As slippage in the pinned connection was considerable compared with the deformations in the core at low-displacement amplitudes, the history was further modified to achieve more uniform displacements in the core. The loading rate was slow. The resulting displacement time history for Brace A is given in Figure 7.

The loading history for the Brace B (Figure 7) was based on the loading history in the Draft *Recommended Provisions for Buckling-Restrained Braced Frames* (BRBF) (SEAONC, 2003). This is similar to that recommended by Sabelli (2004). This loading history is defined by a number of cycles at different levels of displacement ductilities. After the prescribed cycles at increasing displacement amplitude, the specimen was cycled at constant amplitude until failure at the maximum displacement amplitude. The displacements were controlled using the total displacement measured in the actuator. The yield displacement, Δ_y, used to define the loading history was based on the estimated displacement calculated at a 0.2% offset strain, over the core length for Brace A, that is, 0.064 in. No slippage was observed before yielding and thus did not affect the yield displacement. It is important to note that the displacement at 0.2% offset strain was considerably higher than would be estimated if a method

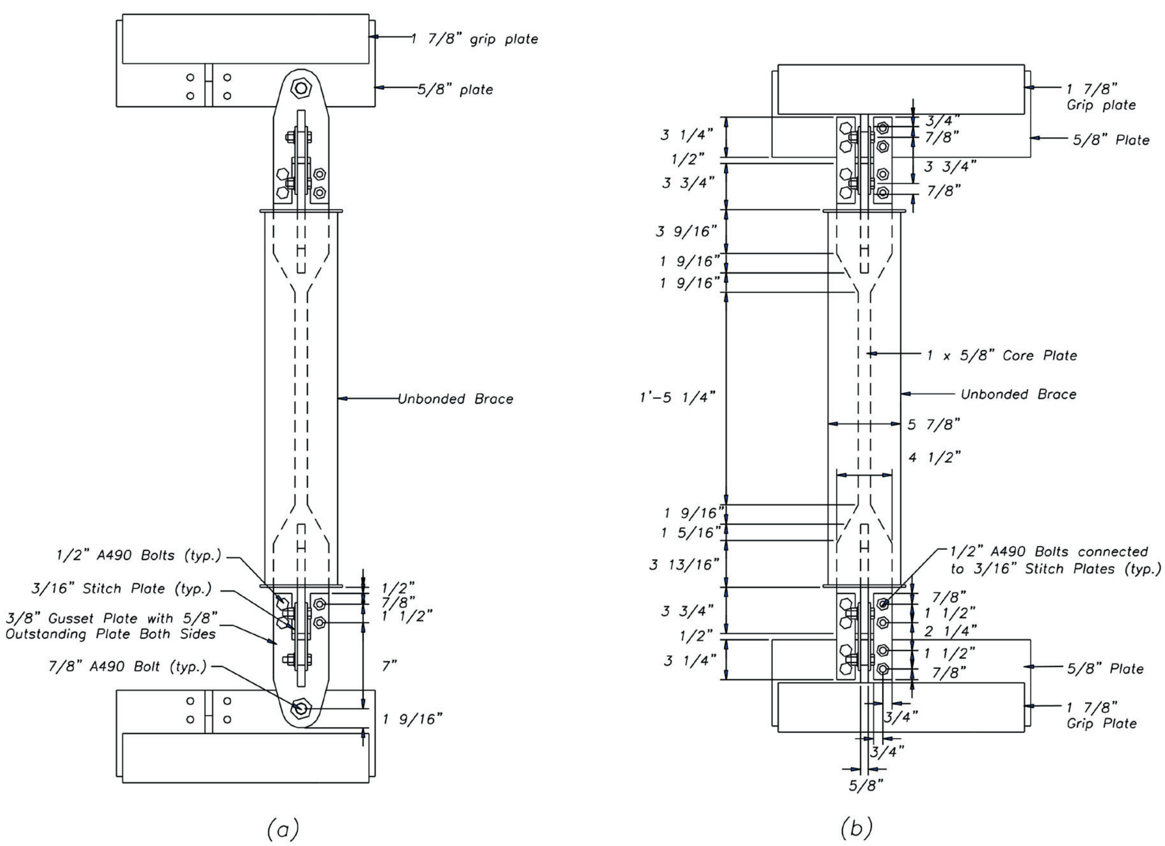

Fig. 4. Buckling-restrained braces setup for axial cyclic experiments with (a) pin-ended connections and (b) moment-resisting, slip-critical connections.

such as the ATC-24 procedure (based on the slope at 75% of the yield force) was used. There is an even larger difference when compared with a theoretical yield displacement using a theoretical yield force and elastic modulus. As the BRBF guidelines (SEAONC, 2003) do not define the way in which the yield displacement is to be estimated, the method that resulted in the more severe displacements, that is, at 0.2% offset strain, was used. The other amplitudes were defined based on this displacement at $2\Delta_y$, $4\Delta_y$, and $6\Delta_y$. The loading history for Brace C (Figure 7) was the reverse of that for Brace B, followed by additional constant amplitude loading until failure applied at a slow rate. For Brace D the same loading history was used (Figure 7) but applied dynamically to the brace at a frequency of 2 Hz to simulate a bridge with a 0.5-s effective period. This was equivalent to a maximum strain rate of 25% per second.

Brace E was the brace first used in the north end of the bridge model (Carden, Itani, and Buckle, 2006b) and had already been subject to some inelastic deformation, although it had not failed. It was subjected to further inelastic behavior using axial cyclic loading with the same loading history as that applied to Brace D, at a dynamic rate of 2 Hz (Figure 8). Brace F was the brace used in the south end of the bridge model and was cycled to failure at constant amplitude of $\pm 3\Delta_y$; with Δ_y as defined previously, at a slow rate (Figure 8).

The final brace, Brace G, was the brace used at the midspan of the bridge model. It was heavily worked in the bridge model and subsequently was subjected to just one cycle $9\Delta_y$ until failure at a slow rate of loading (Figure 8).

CYCLIC BEHAVIOR OF THE BUCKLING-RESTRAINED BRACES

Hysteretic Properties and Connection Slippage

Excluding Brace A, the braces were designed to have slip-critical connections. The displacement time histories in Figures 7 and 8 indicate that where slippage occurred, it sometimes resulted in a large difference between the total displacement in the brace and the displacement measured across the length of the core. As expected, slippage occurred in the pin-ended connections of Brace A, indicated by the large difference in the total and core displacements in Figure 7. In contrast, for other braces such as B and C, there was little difference because slippage was prevented, or in the case of Brace B, delayed until late in the history. Prior to slippage, the small difference between the two measured displacements can be attributed to elastic deformations in the connection region. Slippage was also observed in the dynamically loaded Braces D and E and with the large amplitude displacements in Brace G.

Fig. 5. Buckling-restrained brace with pinned-end connections.

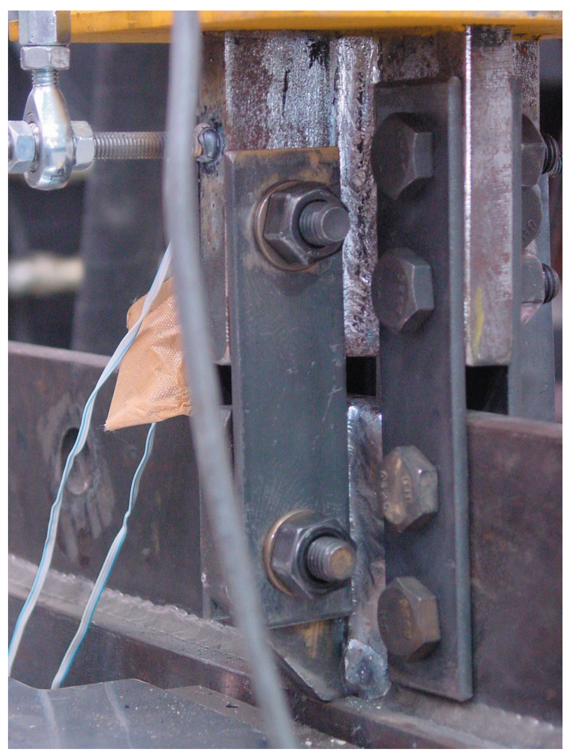

Fig. 6. Buckling-restrained brace with fixed-end connections.

The axial force-displacement curves for each unbonded brace are shown in Figures 9 and 10. Overall, the hysteresis loops exhibit good energy dissipation characteristics and repeatable behavior. The effect of slippage can also be observed in these figures, when comparing the plots for the total displacement with those for the displacement across the core of the brace. The slip force for the slip-critical connections was calculated at 40 kips based on AISC serviceability criteria (AISC, 2001), while the apparent slip force, determined

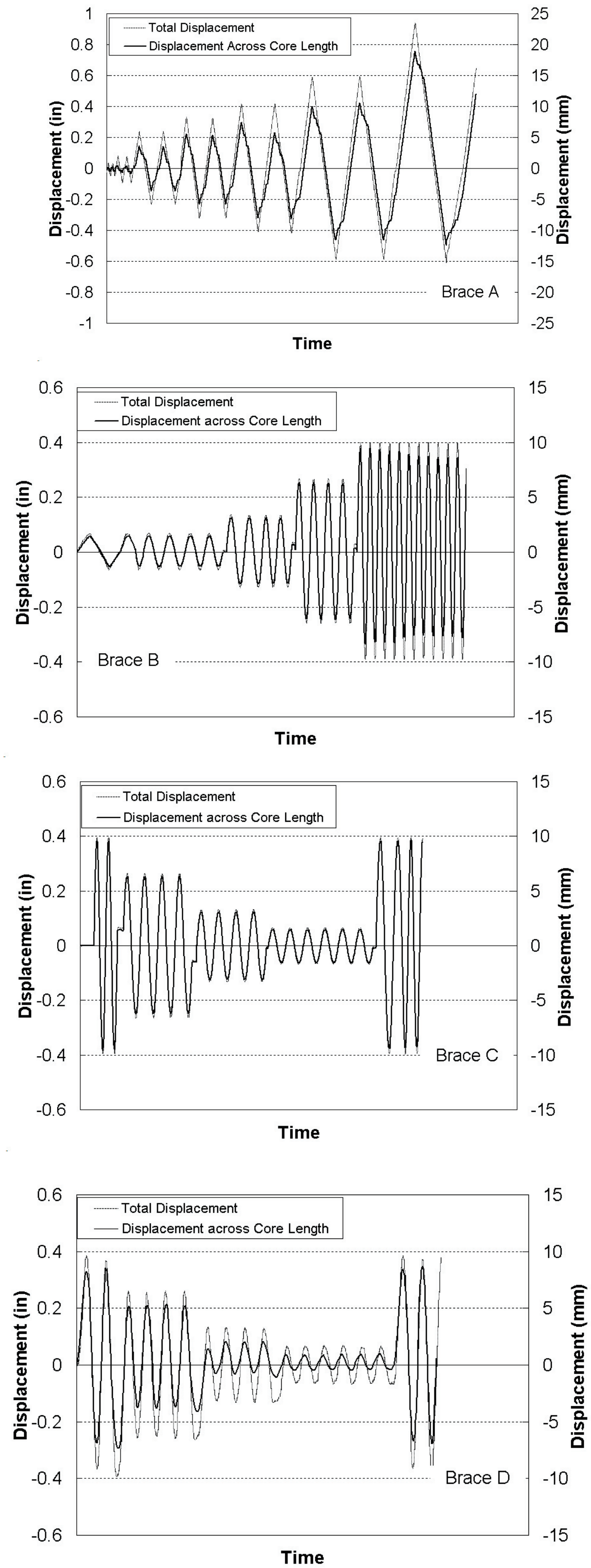

Fig. 7. Axial displacement loading history for Braces A, B, C, and D.

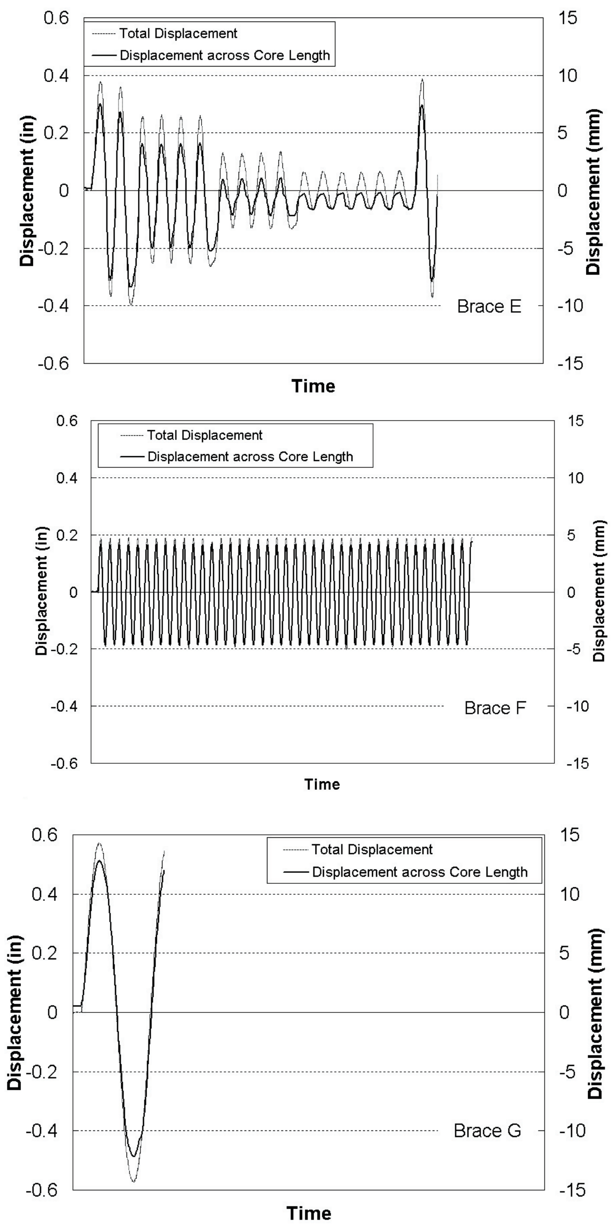

Fig. 8. Axial displacement loading history for Braces E, F, and G in the load frame after being subjected to deformations in the bridge model.

by inspection of the hysteresis loops, was less than this value—at typically around 30 kips. The calibrated wrench pretensioning method is known to result in significant scatter, due to a number of factors described in the *Specification for Structural Joints Using ASTM A325 or A490 Bolts* (AISC, 2001), which is supported by these experimental observations. Another explanation may be that the faying surface, a clean Class A surface, did not provide the friction coefficient assumed in design (0.33).

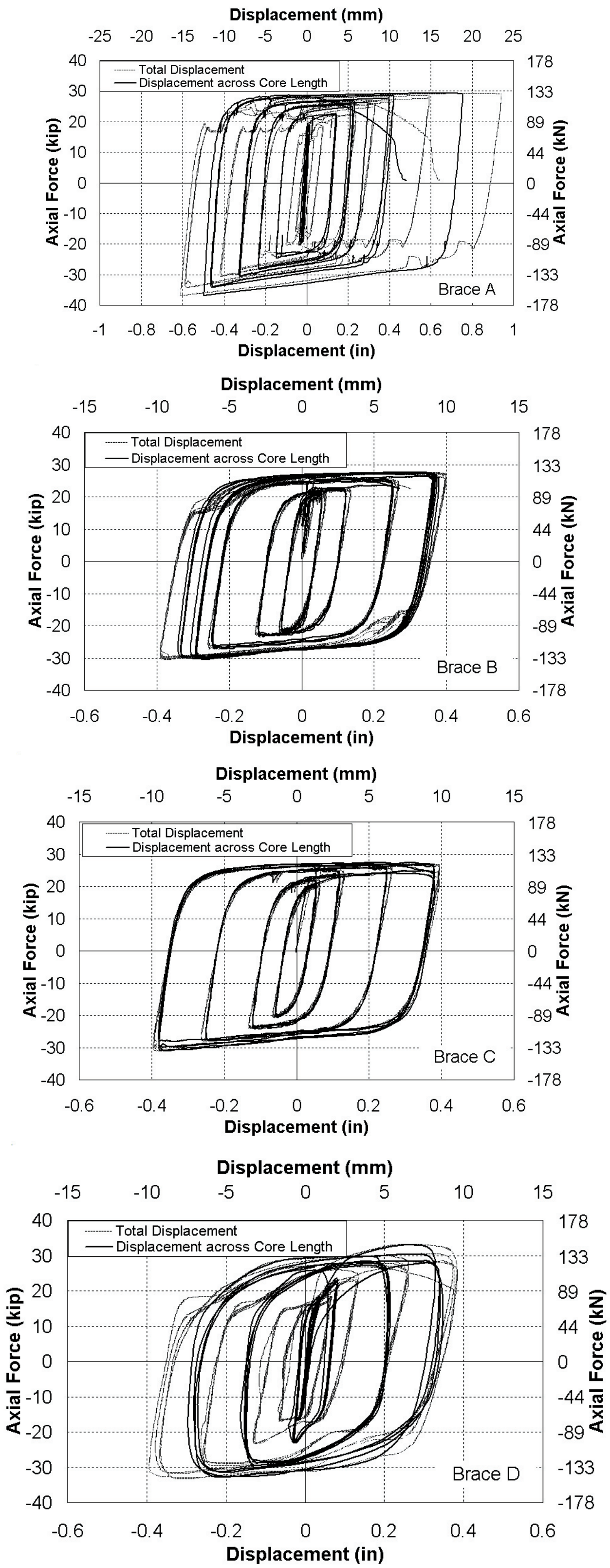

Fig. 9. Force-displacement hysteresis loops for Braces A, B, C, and D.

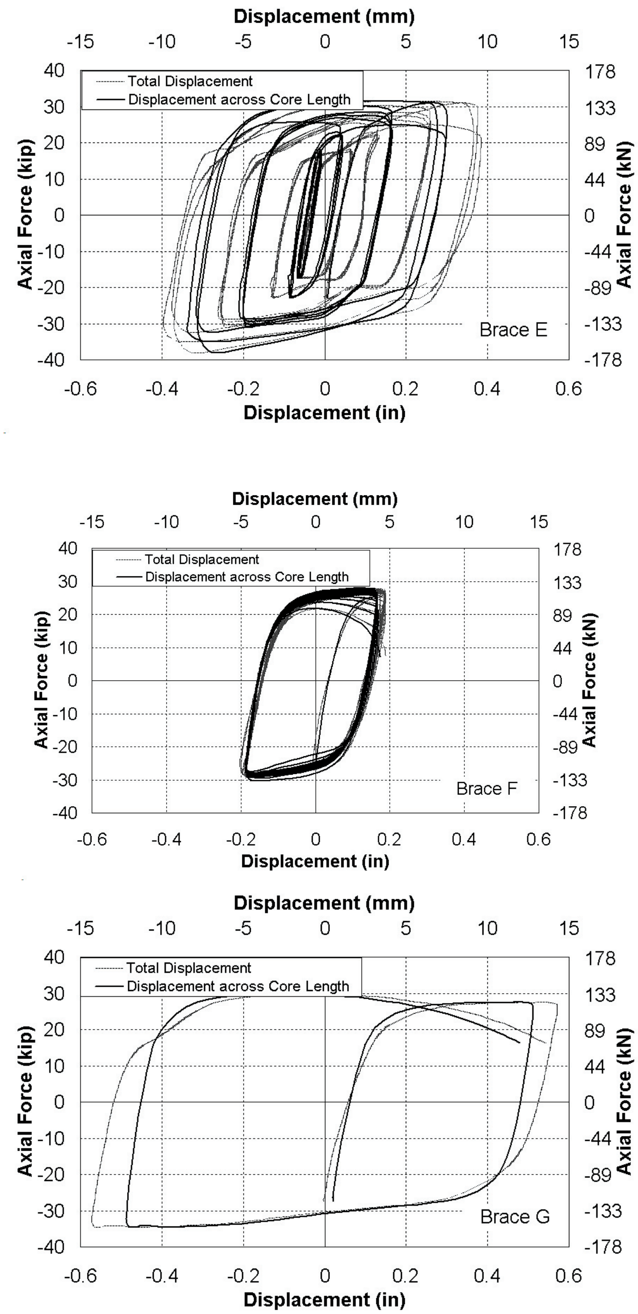

Fig. 10. Force-displacement hysteresis loops for Braces E, F, and G.

Table 1. Maximum Strains and Cumulative Plastic Displacement Capacity of Unbonded Braces

Brace	Loading History	Maximum Strain, %		Cumulative Plastic Strain, %		Cumulative Plastic Ductility	
		Bridge	Load Frame	Bridge	Load Frame	Bridge	Load Frame
A	Modified ATC-24	–	3.71	–	54	–	479
B	BRBF Normal Static	–	1.86	–	98	–	875
C	BRBF Reversed Static	–	1.87	–	66	–	588
D	BRBF Reversed Dynamic	–	1.71	–	38	–	337
E	BRBF Reversed Dynamic[a]	1.76	1.77	41	40	366	352
F	Constant Static[b]	2.22	0.92	23	125	205	1109
G	Constant Static[c]	2.29	2.51	76	22	674	192

[a]Loading history applied in the load frame after the braces were removed from the south end of the bridge model following shake table experiments.

[b]Loading history applied in the load frame after the braces were removed from the north end of the bridge model following shake table experiments.

[c]Loading history applied in the load frame after the braces were removed from the mid-span of the bridge model following shake table experiments.

Maximum and Cumulative Displacements

The maximum displacements, converted to average axial strains in the length of the core for the unbonded braces during each of the component experiments, are given in Table 1. For Braces E, F, and G, which were subjected to deformations in the bridge model, the maximum axial strain observed during these experiments is also given in Table 1. Axial strain is used to define the maximum brace displacements instead of ductility as it is independent of the yield displacement and yield strength and therefore can provide a more consistent measure between braces. The maximum strain in brace A, with increasing amplitude cycles until failure was 3.7%. For the BRBF history (SEAONC, 2003) the maximum strain was approximately 1.9%, although slightly less in cases where slippage occurred.

Cumulative displacement capacity was evaluated for the braces using measures of cumulative plastic strain and cumulative plastic ductility (Table 1). The cumulative plastic strain was calculated by estimating the total plastic axial displacement during a loading history, using a simple algorithm, divided by the effective length of the core (20.4 in.). The cumulative plastic ductility was calculated from the cumulative plastic displacement divided by the yield displacement, included for comparison with previous studies such as Black, Makris, and Aiken (2002). As the yield strength of each of the braces was the same, these two measures were equivalent. Both require an estimation of the yield displacement, which was assumed to be equal to the theoretical yield displacement, Δ_y, over the length of the core plate given by

$$\Delta_y = \frac{F_{ye}L}{E} \tag{1}$$

where

F_{ye} = expected yield strength of the core plate (= 32.6 ksi)
L = length of the core plate (= 20.4 in.)
E = elastic modulus (= 29,000 ksi)

This resulted in a theoretical yield displacement of 0.0229 in. This estimate of the yield displacement was around 29% less than the average yield displacement measured in the braces using the ATC 24 (ATC, 1992) procedure and is approximately 36% of the displacement calculated at the 0.2% offset strain used to define the loading history. The large difference highlights the importance of clearly defining the method in which yield displacement is calculated. The theoretical yield displacement was consistent, computable, and comparable for other systems.

Table 1 shows that the cumulative plastic strains vary greatly between the different specimens with a range between 38 and 148% (when combining the estimated cumulative plastic strains from the bridge excitations and load frame axial deformations). Much of this variation is attributed to the inherent variability of fracture that cannot be easily quantified; however, there are certain factors that can be judged to affect the cumulative plastic strain when comparing the different braces. While the aim was to find a measure of cumulative displacement that was independent of the maximum strain, comparing the braces in Table 1 shows that the braces that were subjected to the smallest strain amplitudes tended to have larger cumulative plastic strains. Comparing Braces B and C with the normal and reversed slowly applied BRBF loading histories resulted in a 35% lower cumulative plastic strain in the brace with reversed loading. This demonstrates that having large amplitude cycles at the beginning of the history reduces the overall cumulative strain capacity compared with increasing amplitude cycles. Furthermore, applying the loading history dynamically, as in Brace D, further reduced the cumulative strain capacity to 39% of that in Brace B. This reduction may be partly due to the increased forces observed in the dynamically loaded specimen, as discussed in the following section, but could also be attributed to slippage that, when dynamic loads were applied, caused a lowering of the displacement capacity. While it is difficult to substantiate conclusions based on only three observations, conservatism suggests that the cumulative displacement capacity for a brace based on increasing amplitude slow cyclic loads should be reduced for a real earthquake where the dynamic reversed loading history is more representative—at least until further research results are available.

From these experiments it is recommended that ductile end cross frames using buckling-restrained braces should be designed for a maximum deformation during an earthquake not exceeding 2.0%. Therefore, to be consistent with the design of isolation systems (AASHTO, 1999) and also the BRBF recommendations (SEAONC, 2003), the maximum considered earthquake strain is no more than 3.0% (1.5 times the design level strain). The maximum strain limit of 3.0% is less than the 3.7% maximum strain measured in the brace with increasing amplitude cycles of loading. Although the braces in the bridge model were not deformed up to strains of 3.7% during shake table experiments, an analytical model of the bridge was used to determine the cumulative plastic strain in the brace for a series of different earthquakes scaled to result in a 3.0% strain in the braces. Resulting cumulative plastic strains for 10 different earthquake excitations are listed in Table 2. The average cumulative plastic strain was 26% and the mean plus one standard deviation cumulative plastic strain was 40%. This is approximately equal to the most conservative value of the cumulative plastic strain (38%) measured in the axial experiments. Therefore, a 3.0% maximum strain is considered an appropriate level for the maximum considered earthquake and 2.0% strain is appropriate for the design level earthquake.

The axial strains in the braces used in ductile end cross frames of bridges can be converted to girder drifts where the girder drift is defined by the lateral displacement in the cross frames divided by the depth of the girders. This enables the displacement limits to be described using the same terms as used in building provisions. However, different girder sizes and configurations will change the axial strain to drift ratio, therefore using axial strain that is directly related to inelastic deformations in the brace as the basis for defining design displacements is more rational. This is synonymous with the specified link rotation limits for eccentrically braced frames in the AISC *Seismic Provisions for Structural Steel Buildings* (AISC, 2002). In addition, the use of axial strain for calculating displacement limits implies the same deformation capacity in lower strength steels than for higher strength steels. If ductility is used as a basis for determining a displacement capacity, the implication is that higher strength steels with equal stiffness have a larger displacement capacity than lower strength steels, when, in fact, the reverse is generally true.

Axial Yield and Ultimate Forces

Two coupon tests were performed on the LYP-225 steel used in the manufacturing of the unbonded braces provided by Nippon Steel (Nippon, 2002). The measured yield strengths (32.3 and 34.1 ksi) were within 5% of the nominal yield strength of 32.6 ksi (225 MPa). Unlike most U.S. steels, where the nominal strength is generally defined so that the majority of specimens are stronger than the nominal strength, the nominal strength for the LYP-225 steel is defined in the middle of a relatively tight range (29.7 to 35.5 ksi) of acceptable yield strengths. Therefore, the nominal strength of 32.6 ksi was assumed to be the expected strength for this material. The ultimate strength of the LYP-225 steel was around 35% higher than the yield strength. The ultimate strain was much higher at around 65% for the LYP-225 steel compared with typical values of 30 to 35% for A36 steel (Carden, Itani, and Buckle, 2006c).

The expected yield force for the unbonded braces, P_{ye}, was defined as

$$P_{ye} = F_{ye} A_{sc} \tag{2}$$

Table 2. Cumulative Plastic Strains and Ductilities in Braces from an Analytical Model of a Bridge Subjected to Different Earthquakes Resulting in a Maximum Brace Strain of 3.00%

Earthquake	Station and Component	Amplitude Scale Factor	Maximum Brace Strain, %	Cumulative Plastic Strain, %	Cumulative Plastic Ductility
1940 Imperial Valley	El Centro Array#9 NS	2.80	3.04	37.1	286
1966 Parkfield	California Array#2 NS	1.50	3.05	20.1	155
1971 San Fernando	Pacoima Dam NS	1.75	2.94	28.4	219
1977 Bucharest	Building Res. Inst. NS	3.70	3.00	18.3	141
1979 Imperial Valley	Array #7 230˚	1.60	3.12	21.8	168
1992 Landers	Lucerne EW	2.50	2.93	13.7	106
1994 Northridge	Sylmar Hospital NS	1.10	3.00	11.8	91
	Rinaldi 229˚	0.80	2.95	13.1	101
1995 Kobe	KJMA NS	1.30	2.94	46.3	357
1999 Taiwan Chi-Chi	TCU084 EW	0.80	3.13	49.2	380
Average			3.01	26.0	200
Average + 1 Standard Deviation			3.08	39.7	307

where

F_{ye} = expected yield strength (= 32.6 ksi)
A_{sc} = area of the steel core (= 0.625 in.^{2})

Thus the expected yield force was equal to 20.4 kips. The yield force for each unbonded brace was estimated using the force at a 0.2% offset strain and was found for each brace. Table 3 lists the measured yield force for each unbonded brace and shows that they were slightly larger than the expected yield forces but within 12% for all braces.

The overstrength factor, ω, which describes the maximum tensile force measured in the brace divided by the expected yield strength, was calculated for each brace and is given in Table 3. The ω factor was generally around 1.35, similar to the difference between the yield and ultimate strengths measured in the coupon tests. The overstrength factor was larger in some instances, such as Brace D, which had the largest overstrength factor. This is attributed to the high strain rate in experiments on Brace D that increased the force in the brace, particularly during the first cycle of the loading. This can be observed in Figure 9 when comparing the response to the same loading history applied slowly for Brace C and dynamically for Braces D and E. Brace D had no previously applied deformations and the resulting maximum force in the first cycle was 30% larger than the corresponding force in the first cycle of Brace C. However, the strain rate effect was most pronounced in the first cycle of loading as subsequent cycles stabilized to around a 10 to 15% difference when comparing Braces C and D. Brace E had been previously loaded in the bridge model and, as a result, the first cycle of loading was not as high as that in Brace D, although each cycle exhibited maximum forces around 15% higher than in Brace C. Braces A and G, which had larger maximum strains in the core than the other braces, also exhibited ω factors greater than 1.35.

The compression strength adjustment factor, β, is defined as the maximum compression force divided by the maximum tension force, and is calculated and listed in Table 3 for each of the braces. The compression strength adjustment factor was typically around 1.10 to 1.15, indicating a maximum compression force 10 to 15% larger than the tension force. Thus, β was largest for the braces with the largest maximum strains as shown for Braces A and G, while the reverse is true for smaller strains as in Brace F, indicating that the compression overstrength tended to increase as the core strain increased. This is attributed to high mode buckling and the Poisson effect causing increased friction between the core and the surrounding encasement at high strains. For Brace D the maximum compression force was actually less than the maximum tension force due to a large observed tension force

Table 3.Yield and Maximum Tension and Compression Forces in the Unbonded Braces

Brace	Loading History	Expected Yield Force, kips	Measured Yield Force, kips	Maximum Tension Force, kips	Maximum Compression Force, kips	Overstrength Factor, ω	Compression Strength Adjustment Factor, β
A	Modified ATC-24	20.4	21.6	29.3	–36.9	1.44	1.26
B	BRBF Normal Static		21.1	27.7	–30.6	1.36	1.11
C	BRBF Reversed Static		22.7	27.4	–31.0	1.35	1.13
D	BRBF Reversed Dynamic		22.8	33.0	–32.7	1.62	0.99
E	BRBF Reversed Dynamic[a]		21.7	31.5	–37.6	1.55	1.19
F	Constant Static[b]		21.7	28.0	–30.3	1.37	1.08
G	Constant Static[c]		22.0	30.0	–34.6	1.47	1.15

[a]Loading history applied in the load frame after the braces removed from the south end of the bridge model following shake table experiments.
[b]Loading history applied in the load frame after the braces removed from the north end of the bridge model following shake table experiments.
[c]Loading history applied in the load frame after the braces removed from the mid-span of the bridge model following shake table experiments.

in the first reversal of the dynamically loaded specimen.

Energy Dissipation in the Unbonded Braces

The area enclosed by each hysteresis loop was calculated for Braces A through D at different cycles of loading during the component experiments. The displacement was based on that measured across the core length. The hysteretic area was compared with the circumscribing rectangle defined by the maximum positive and negative forces and displacements ("ideal" area). The normalized energy dissipated per cycle is plotted against maximum axial strain amplitude for each cycle in Figure 11. This figure demonstrates that once significant yielding had occurred, the area inside the hysteresis loop was typically around 80% of the rectangular area. This is much higher than the same ratio for concentric braces, such as single angle braces, which exhibit buckling and elongation (Carden et al., 2006c). Unlike the situation for the single angles, the effective energy dissipation by the buckling-restrained braces increased as the displacement amplitude increased. Hence these braces were much more efficient than the single angles for energy dissipation, imply-

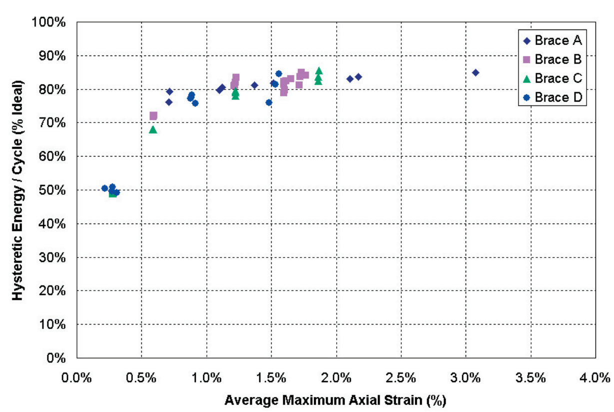

Fig. 11. Energy dissipated per cycle as a ratio of "ideal" for Braces A, B, C, and D.

ing that there should be smaller drifts in ductile end cross frames that use buckling-restrained braces compared with those that use single angles for the same level of forces, as was observed by Carden et al. (2006c).

The hysteretic energy reported in Figure 11 is based on the displacements across the core length. It might be expected that slippage in the connections would reduce the effective energy dissipated per cycle. To quantify this effect, the hysteretic energy dissipated per cycle was calculated based on the total displacements in the brace including the connections for a hysteretic area based on the total brace displacements including the connections for Brace A, the brace exhibiting the most slippage with the pinned-end connections. It was found that the measured energy dissipation as a ratio of circumscribing area was reduced by around 5% at any given level of strain, thus connection slippage had a relatively small effect on the efficiency of the brace. Consequently, in terms of energy dissipation there is no apparent advantage in providing slip-critical connections in unbonded braces for seismic loading.

Strain Gage Readings

Strain gages were placed on Braces A and B, with gages on either side of the core plate near each end of the core length. A typical strain gage measurement in Brace B is plotted against the axial force in Figure 12. This figure shows that there are both tensile and compressive plastic strains in the brace, although there is some bias toward tensile strains. This can be explained by the higher mode buckling that is known to occur in the core section of buckling-restrained braces. Consequently, the maximum measured strain was higher, at 4.83%, compared with the maximum average computed strain from the displacement across the core of the brace of 1.86%. Brace A shows similar strains, indicating that the pinned-end connection did not adversely affect the localized strains.

While in the elastic range, the strain gages were used to estimate the forces in the unbonded brace using the elastic modulus, assumed to be equal to 29,000 ksi, and the area of the core plate. Good correlation was shown between the measured and computed axial forces, where the difference between the two was less than 8%, demonstrating that the gages could be used to monitor elastic force levels in the braces after installation in a bridge.

ANALYTICAL MODEL

Black et al. (2002) showed that the hysteretic properties of a buckling-restrained brace can be captured well with a Bouc-Wen model (Wen, 1976). However, for design using such methods as a capacity spectrum analysis, it is more useful to characterize the behavior using a bilinear model, although some loss of accuracy is expected. A bilinear model was shown to fit the experimental data reasonably well. The initial stiffness, K_i, was calculated based on the cross-sectional properties of the core and the core length, giving an initial stiffness of 889 kip/in. The post-yield stiffness ratio, α, was assumed to be equal to 0.025 in order to fit the backbone curve for the increasing amplitude cyclic displacements. The yield force was assumed to be equal to the expected yield of 20.4 kips for the static cases, and was amplified by 15% to 23.5 kips for the dynamically loaded braces.

The analytical model was subjected to the same displacement time history as the axial cyclic experiments. The resulting hysteresis loop for Brace B, as an example, is shown in Figure 13. The bilinear model is shown to fit the cyclic backbone curve for the experimental data well, although it was conservative for the response in compression. Without a separate model for the tension and compression properties,

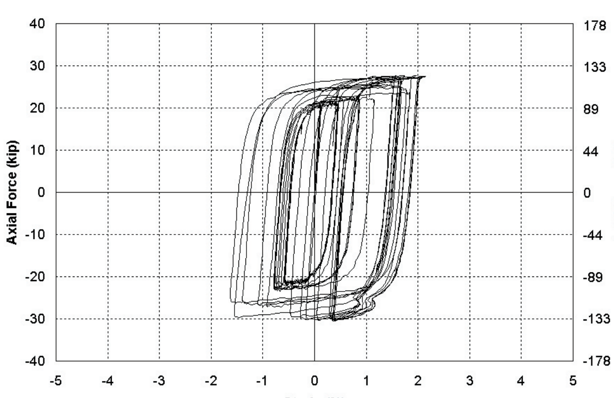

Fig. 12. Typical strain gage measurement for Brace B.

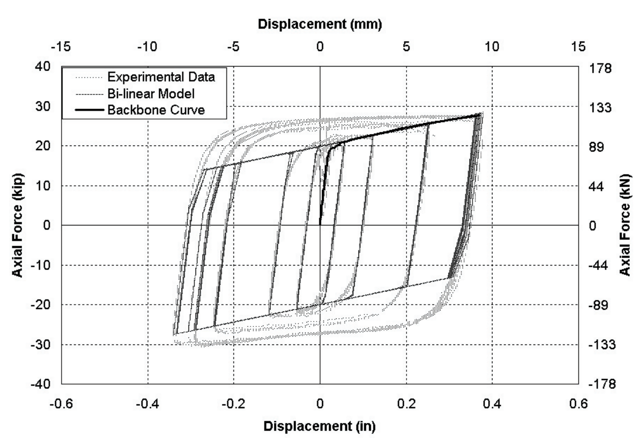

Fig. 13. Analytical hysteresis loop compared with backbone curve and experimental data for Brace B.

this is unavoidable. The dynamic strain rate effect is evident in Brace D. However, increasing the yield force by 15% resulted in a reasonable comparison between the experimental and analytical results. This was the basis for the inelastic properties of the analytical bridge model used to calculate cumulative displacement responses described in the earlier section.

While the bilinear model captures the elastic loading and unloading and cyclic backbone curve of the unbonded braces well, it loses some accuracy in modeling the initial reversal and post-yield stiffness of an individual cycle of loading in the braces, as observed in Figure 13. The main effect of this is a difference in the area inside the hysteresis loops. A comparison of the hysteretic energy dissipated per cycle for the experimental data and the bilinear model shows that the hysteretic areas are similar at moderate strains, but larger differences are observed at higher amplitudes. At strains of around 2%, the bilinear model typically underestimates the energy dissipation by around 20%, making the bilinear analytical response conservative.

CONCLUSION

The cyclic inelastic behavior of buckling-restrained braces was studied for potential implementation in ductile end cross frames at the supports of steel plate girder bridges. The unbonded braces exhibited excellent hysteretic behavior with similar properties in tension and compression. Slippage in the connections was observed in some of the braces, although this did not have a significant effect on the energy dissipation characteristics of the braces. The braces were subjected to different loading histories with displacements up to an equivalent axial strain in the core of the brace of 3.7%. Various loading histories show that a history with large amplitude cycles at the beginning followed by smaller cycles, like a typical earthquake loading history, tends to result in lower cumulative plastic strain capacity than an increasing amplitude history. Dynamic loading also lowers the cumulative plastic strain capacity compared with static loading, which is attributed to increased forces during dynamic loading and also the dynamic effects of slippage.

The yield tension force of the unbonded braces is within 12% of that predicted. The maximum forces due to strain and cyclic hardening at a design strain of 2% are typically 35% greater than the expected yield strength. Dynamic loading increases these forces by typically 15% and up to 30% for the first cycle of loading. The maximum compression force is generally 10 to 15% greater than the tension force. The area of the hysteresis loops for the unbonded braces is around 80% of the circumscribing rectangular area and increases as strains increase unlike the degradation seen in typical concentric braces after buckling. The response of the braces can be approximately modeled with a bilinear representation to capture the maximum forces, displacements and, more conservatively, the energy dissipation in the braces.

From this study it is recommended that a maximum brace strain of 2.0% be used for design of the buckling-restrained braces when used in ductile end cross frames. Results from an analytical study of a bridge model showed for 10 earthquakes that the mean plus one standard deviation cumulative plastic strain demand, for maximum displacements of 1.5 times the design displacement, was equal to the lowest cumulative plastic strain capacity measured during experiments.

ACKNOWLEDGMENTS

This project was funded by the Federal Highway Administration through the Highway Project at the Multidisciplinary Center for Earthquake Engineering, University of Buffalo under contract DTFH61-98-C-00094. Additional funding was provided by the California Department of Transportation under contract 59Y564. Grateful acknowledgment is made of both agencies for their generous support. The donation of the unbonded braces by Nippon Steel Corporation and assistance of Dr. Ian Aiken in facilitating these experiments is also greatly appreciated.

REFERENCES

American Association of State Highway and Transportation Officials (AASHTO) (1999), *Guide Specifications for Seismic Isolation Design,* Second Edition including 2000 Interim Revisions, AASHTO, Washington, DC.

AISC (2001), *Load Factor and Resistance Design Manual of Steel Construction*, 3rd Edition, American Institute of Steel Construction, Inc., Chicago, IL.

AISC (2002), *Seismic Provisions for Structural Steel Buildings*, American Institute of Steel Construction, Inc., Chicago, IL.

ATC (1992), *ATC 24–Guidelines for Cyclic Seismic Testing of Components of Steel Structures*, Applied Technology Council, Redwood City, CA.

Astaneh-Asl, A., Bolt, B., McMullin, K.M., Donikian, R.R., Modjtahedi, D., and Cho, S. (1994), *Seismic Performance of Steel Bridges During the 1994 Northridge Earthquake*, UCB/CE-STEEL-94/01, Department of Civil Engineering, University of California at Berkeley, Berkeley, CA.

Black, C., Makris, N., and Aiken, I. (2002), *Component Testing, Stability Analysis and Characterization of Buckling Restrained Unbonded Braces,*™ Technical Report: PEER 2002/08, Berkeley, CA.

Bruneau, M., Wilson, J.W., and Tremblay, R. (1996), "Performance of Steel Bridges during the 1995 Hyogoken-Nanbu (Kobe, Japan) Earthquake," *Canadian Journal of Civil Engineering*, Vol. 23, No. 3, pp. 678–713.

Carden, L.P., Itani, A.M., and Buckle, I.G. (2006a), "Seismic Performance of Steel Girder Bridges with Ductile Cross Frames Using Single Angle X Braces," ASCE, *Journal of Structural Engineering*, Vol. 132, No. 3, March 1.

Carden, L.P., Itani, A.M., and Buckle, I.G. (2006b), "Seismic Performance of Steel Girder Bridges with Ductile Cross Frames using Buckling-Restrained Braces," ASCE, *Journal of Structural Engineering*, Vol. 132, No. 3, March 1.

Carden, L.P., Itani, A.M., and Buckle, I.G. (2006c), "Cyclic Behavior of Single Angles for Ductile End Cross Frames in Steel Girder Bridges," AISC, *Engineering Journal*, Vol. 43, No. 1, 4th Quarter.

Clark, P.W., Aiken, I.D., Tajirian, F.F., Kasai, K., Ko, E., and Kimura, I. (1999), "Design Procedures for Buildings Incorporating Hysteretic Damping Devices," *International Post-SMiRT Conference Seminar on Seismic Isolation, Passive Energy Dissipation and Active Control of Vibrations of Structures*, Cheju, Korea, August 23–25.

Kim, J. and Choi, H. (2004), "Behavior and Design of Structures with Buckling-Restrained Braces," *Engineering Structures*, Vol. 26, pp. 696–706.

Lopez, W.A., Gwie, D.S., Lauck, T.W., and Saunders, C.M. (2004), "Structural Design and Experimental Validation of a Buckling-Restrained Braced Frame System," *Engineering Journal*, Vol. 41, No. 4, pp. 177–186.

Nippon (2002), *Seismic Behavior of Typical Steel (Unbonded Brace)—Tensile Test Report for Steel Material of LYP-225*, Report: Nippon Steel Corporation, Japan.

Sabelli, R. (2001), *Research on Improving the Design and Analysis of Earthquake-Resistant Steel-Braced Frames*, Technical Report: PF2000-9–FEMA/EERI 2000 Professional Fellowship, Oakland, CA.

Sabelli, R. (2004), "Recommended Provisions for Buckling-Restrained Braced Frames," *Engineering Journal*, Vol. 41, No. 4, pp. 155–175.

SEAONC (2003), *Recommended Provisions for Buckling-Restrained Braced Frames*, Structural Engineering Association of Northern California, Sacramento, CA, July.

Shinozuka, M.(ed.), Ballantyne, D., Borcherdt, R., Buckle, I., O'Rourke, T., and Schiff, A. (1995), *The Hanshin-Awaji Earthquake of January 17, 1995 Performance of Lifelines*, Technical Report: NCEER-95-0015, National Centre for Earthquake Engineering Research, Buffalo, NY.

Wada, A., Saeki, E., Takeuchi, T., and Watanabe, A. (1989), "Development of Unbonded Brace," *Column (A Nippon Steel Publication)*, No 115, p. 12.

Wen, Y.-K. (1976), "Method for Random Vibration of Hysteretic Systems," *Journal of Engineering Mechanics*, Vol. 102(EM2), pp. 249–263.

Zahrai, S.M., and Bruneau, M. (1998), "Impact of Diaphragms on Seismic Response of Straight Slab-on-Girder Steel Bridges," *Journal of Structural Engineering*, Vol. 124, No. 8, pp. 938–947.

Zahrai, S.M. and Bruneau, M. (1999), "Cyclic Testing of Ductile End-Diaphragms for Slab-on-Girder Steel Bridges," *Journal of Structural Engineering*, Vol. 125, No. 9, pp. 987–996.